# Subduction zone anisotropy beneath Corvallis, Oregon: A serpentinite skid mark of trench-parallel terrane migration?

Jeffrey Park, Huaiyu Yuan,[1] and Vadim Levin[2]

Department of Geology and Geophysics, Yale University, New Haven, Connecticut, USA

Received 1 August 2003; revised 12 August 2004; accepted 20 August 2004; published 16 October 2004.

[1] We studied the back azimuth dependence of *Ps* converted phases at GSN station COR (Corvallis, Oregon) using broadband *P* receiver functions computed from 602 teleseismic earthquakes. The amplitudes and polarities of the transverse *Ps* phases are largely two-lobed, which indicates anisotropy with a tilted symmetry axis. A double-peaked *Ps* conversion at 4.5–6.5 s delay has the moveout of a dipping slab but is not consistent with simple deflection of the *Ps* converted phase by the dipping interface. A polarity flip on the transverse receiver function near north-south back azimuth indicates an anisotropic symmetry axis aligned north-south, far from the convergence direction (N68°E). The *Ps* phase is modeled using reflectivity synthetics with a highly anisotropic layer of depressed wave speed ($V_P \sim 6.0$–$6.5$ km/s) near 40 km depth, at the slab interface with the overriding North American plate. One-dimensional modeling suggests 10% anisotropy in the supraslab layer, with a slow symmetry axis oriented N5°W at a 60° tilt from the vertical. Adjustments for the effect of slab interface dip on *Ps* amplitude suggest a somewhat lower 7% anisotropy. We infer a thin (~7 km) anisotropic detachment zone for the northward slippage of the Siletz forearc terrane along the top of the descending slab, a motion consistent with GPS measurements and models of regional lithospheric dynamics. Serpentinite is a likely constituent for the deep anisotropic layer, owing to its reduced $V_P$ and high Poisson ratio. The ductile rheology and hydrated composition of serpentinite make it a plausible lithology for a mechanical detachment zone. *INDEX TERMS:* 3909 Mineral Physics: Elasticity and anelasticity; 7203 Seismology: Body wave propagation; 7218 Seismology: Lithosphere and upper mantle; 8150 Tectonophysics: Plate boundary—general (3040); 8159 Tectonophysics: Rheology—crust and lithosphere; *KEYWORDS:* anisotropy, Cascadia, subduction

**Citation:** Park, J., H. Yuan, and V. Levin (2004), Subduction zone anisotropy beneath Corvallis, Oregon: A serpentinite skid mark of trench-parallel terrane migration?, *J. Geophys. Res.*, *109*, B10306, doi:10.1029/2003JB002718.

## 1. Introduction: Cascadia Deformation, Receiver Functions, and Anisotropy

[2] The pattern of seismic anisotropy in the Pacific Northwest should reflect its tectonics (Figure 1). On a large scale, paleomagnetic and geobarometric evidence indicates that the coastal terranes of western North America have translated northward by thousands of kilometers during the Cenozoic [*Beck et al.*, 1981; *Irving et al.*, 1985, 1995; *Beck*, 1989; *Butler et al.*, 1989; *Ague and Brandon*, 1992, 1996]. On a regional scale, the oblique subduction of the Juan de Fuca plate has caused complex effects on the continental margin of the northwest United States and British Columbia [*Yeats et al.*, 1996]. A clockwise north migration (relative to the North American plate) of the Cascadia forearc has been proposed by *Beck* [1984], *Wells* [1990], *Wang* [1996], and *Wells et al.* [1998].

[3] New evidence from continuous GPS networks [*Dragert and Hyndman*, 1995; *Khazaradze et al.*, 1999] argue that the southern portion of the Siletz terrane is moving northward at 3–7 mm/yr, causing the forearc terrane to shorten beneath western Washington and induce elevated crustal seismicity rates in the Puget Sound region [*Mazzotti et al.*, 2002]. Although terrane migration is typical for oblique subduction, *McCaffrey et al.* [2000] argues that northward terrane migration in Cascadia is driven primarily by gravitational collapse of elevated Basin and Range topography. Mounting evidence for intraterrane deformation is puzzling in light of the region's low level of moderate seismicity, which might otherwise delineate the shear zones associated with the deformation. The mystery deepens when one considers recent reports of periodic slow earthquakes in the Cascadia subduction zone that have minimal seismic radiation [*Miller et al.*, 2002].

[1]Now at Department of Geology and Geophysics, University of Wyoming, Laramie, Wyoming, USA.

[2]Now at Department of Geological Sciences, Rutgers University, Piscataway, New Jersey, USA.


0148-0227/04/2003JB002718$09.00

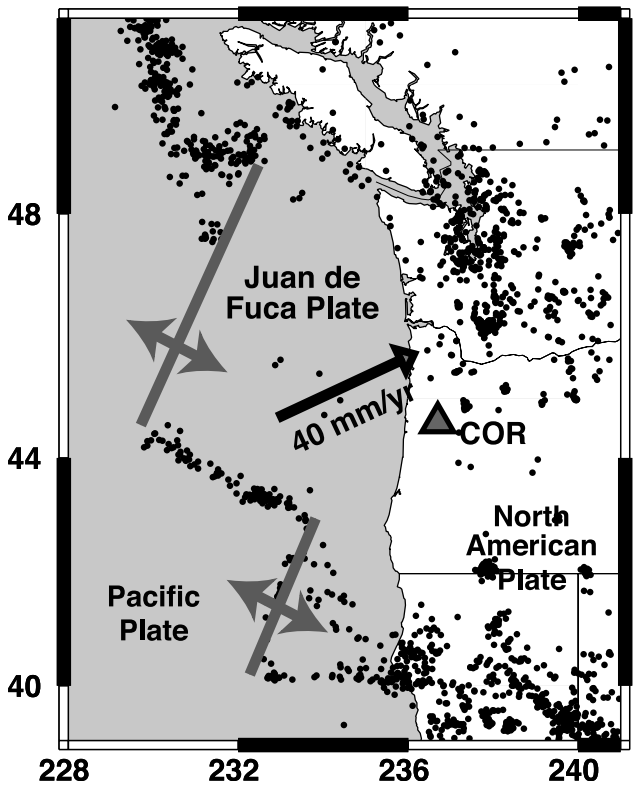


**Figure 1.** Regional seismicity map for station Corvallis (COR) of the Global Seismographic Network. Symbols denote earthquakes from the catalogs of different organizations, all with magnitude >4.0. Events are numerous in the north and south of the Cascadia subduction zone, and scarce under the Coast Range of Oregon. See color version of this figure in the HTML.

[4] Cascadia tectonic models motivate the study of crust and upper mantle anisotropic structure in the Juan de Fuca subduction zone beneath station COR (Corvallis, Oregon) of the Global Seismographic Network. Anisotropic layering enhances *P*-to-*S* converted phases in teleseismic *P* coda. Receiver functions (RFs) deconvolve the earthquake source from the *P* coda [*Langston*, 1977a, 1981; *Ammon*, 1991; *Park and Levin*, 2000] to reconstruct the *Ps* converted phases and retrieve near-receiver layering in elastic properties. Anisotropic layering in the crust and shallow mantle has been identified from back azimuth variation of *Ps* amplitude, in the transverse component receiver function [*Bostock*, 1997, 1998; *Levin and Park*, 1997b, 2000; *Savage*, 1998]. Several *Ps* conversions are evident in the COR receiver functions, consistent with horizontal zones of localized shear and inconsistent with a common alternative model: dipping interfaces within isotropic material. *Ps* amplitude variations with back azimuth rule out a simple interpretation in which shear aligns with the azimuth of subduction. Rather, inferred shear above the downgoing slab aligns more with the presumed northward migration of the coastal forearc terrane.

[5] Because COR has been collecting data for more than a decade, we were able to use more than 600 teleseismic *P* waves to obtain unprecedented resolution of receiver function variation with the back azimuth of the arriving waves. By using reflectivity synthetics, we tested hypothetical anisotropic structures against the COR RFs by trial-and-error forward modeling. Several models related to potential subduction zone processes are contrasted in section 4. Section 5 contrasts our results with those obtained from *SKS* birefringence and $P_n$ tomography. Section 6 discusses the interpretive trade-offs that suggest the presence of supraslab serpentinite beneath COR. Section 7 summarizes our findings.

## 2. Pacific Northwest Tectonic Setting

[6] Under Washington, central Oregon and northern California, Cascadia subduction is oblique (40–50 mm/yr at N68°E) [*Riddihough*, 1984; *Engebretson et al.*, 1984]. Offshore Washington and central Oregon, the subducting Juan de Fuca plate is young, buoyant and covered by as much as 3 km of terrigenous sediment [*McCaffrey and Goldfinger*, 1995]. As a result, no topographic trench marks the deformation front of the Cascadia subduction zone. The basement rocks throughout the outer arc high are thought to be Paleocene and early Eocene basaltic oceanic crust that accreted to the North America plate about 50 Ma. *Trehu et al.* [1994] refers to the forearc as the Siletz terrane. Active source seismic studies have characterized the Siletz terrane as mafic in character, even at its thickest expression along the Oregon coast, reflecting either a burst of volcanism similar to the formation of an oceanic plateau [*Trehu et al.*, 1994], or else the accretion of successive layers of normal oceanic crust by underplating [*Hyndman et al.*, 1990].

[7] Wadati-Benioff zone seismicity under the Coast Range [*Tabor and Smith*, 1985] shows a shallow dip (10°–15°) for the subducting slab. Seismic reflection and potential field surveys confirm the shallow dip under the Coast Range [*Keach et al.*, 1989; *Trehu et al.*, 1994; *Couch and Riddihough*, 1989]. Farther inland, seismic tomography indicates that the slab steepens to ~65° beneath the Cascade Range and descends to at least 200 km [*Michaelson and Weaver*, 1986; *Rasmussen and Humphreys*, 1988; *Harris et al.*, 1991]. Using receiver functions, *Langston* [1981] identified a 10°–20° east dipping interface that descends inland to 140–150 km as the oceanic Moho of the Juan de Fuca plate. The RFs also suggest that the slab interface steepens under the Cascades, with dip ~50°. In the model of *Li and Nabelek* [1996], the Juan de Fuca Moho dips eastward 11° beneath the Coast Range and steepens to 19° beneath the Willamette Valley. The estimated depth of the subducted Moho beneath station COR is consistent among different studies: *Burdick and Langston* [1977], 45 km; *Trehu et al.* [1994], 45–50 km; *Li* [1996], 40–43 km. *Rondenay et al.* [2001] inverted scattered waves, associated with teleseismic *P* waves, recorded near Corvallis by a portable broadband linear array in 1993–1994, using data previously analyzed by *Li* [1996]. *Rondenay et al.* [2001] traces the Juan de Fuca oceanic crust as a low-velocity channel that seems to lose its velocity signature as it passes under COR. *Bostock et al.* [2002] argues that eclogitization of the oceanic crust erases its low-velocity signature and that metamorphic dehydration of the slab inland of COR serpentinizes the overlying mantle wedge and forms another low-velocity zone at the base of the North American crust.

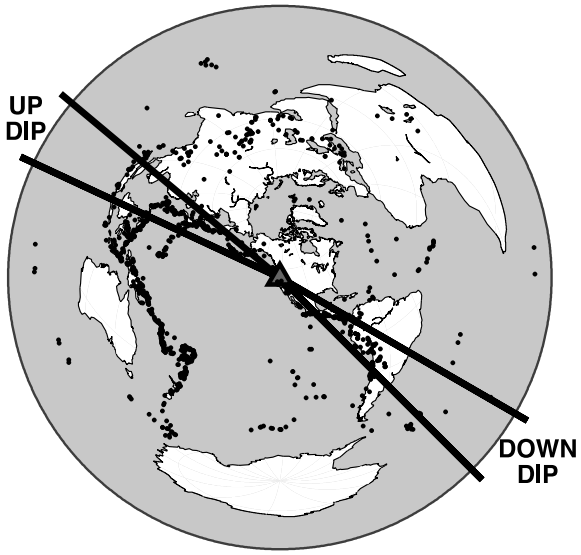


**Figure 2.** Event distribution for the 602 events used in this receiver function study are plotted with dots in a polar map projection centered on station COR (Corvallis, Oregon). Updip and downdip back azimuth sectors, used for epicentral RF sweeps, are marked. See color version of this figure in the HTML.

[8] Certain aspects of the slab dehydration scenario can be addressed with a receiver function study at a long running permanent seismic station like COR. Both receiver functions and the scattering inversion of *Rondenay et al.* [2001] use *P*-to-*S* converted phases in teleseismic *P* coda, but RF estimation can use higher-frequency data and therefore achieve finer resolution in depth. The scattered wave method offers two-dimensional (2-D) resolution by utilizing a linear array of stations, but its current formulation does not include anisotropic effects [*Bostock et al.*, 2001; *Schragge et al.*, 2001]. Serpentinite is often anisotropic [*Kern et al.*, 1997, 2002], and anisotropy appears to have a strong influence on *Ps* converted wave amplitude at COR.

## 3. Observations of *Ps* Converted Phases Beneath Station COR

[9] We retrieved data from station COR (Corvallis, Oregon) of the Global Seismographic Network (GSN) from 1990 to 2000 for earthquakes with $M_S \geq 6.0$ from the IRIS Data Management Center (DMC). We selected 602 broadband three-component teleseismic records for receiver function analysis with the multitaper correlation (MTC) RF estimator described by *Park and Levin* [2000]. Most of these records are of earthquakes with magnitude greater than $M_S = 6.3$. Some events with lower magnitude ($6.0 \leq M_S \leq 6.3$) but high signal-to-noise ratio are also used. The event coverage (Figure 2) is fairly good, with its largest gap in the 180°–210° back azimuth sector.

[10] We estimated receiver functions with a variant of spectral division based on multitaper correlation (MTC) [*Park and Levin*, 2000] to compute frequency domain RFs $H_R(f)$, $H_T(f)$. Multitaper spectrum estimation techniques are resistant to spectral leakage [*Thomson*, 1982; *Park et al.*, 1987], so that the MTC RF estimate exploits low-amplitude portions of the *P* wave spectrum that may nonetheless have high signal-to-noise ratio. We average RF estimates in the frequency domain, weighted by their uncertainties, in overlapping bins of back azimuth (10° bins) and epicentral distance (6° bins). An inverse Fourier transform obtains the time domain RFs $H_R(t)$, $H_T(t)$ from the bin-averaged $H_R(f)$, $H_T(f)$. A cosine-squared low-pass filter is applied in the frequency domain to avoid Gibbs effect ringing. We set the low-pass frequency cutoff in our analysis to 1 Hz, with half amplitude at 0.5 Hz. This frequency limit is chosen to reduce the destructive interference associated with averaging RFs from *P* waves over a range of epicentral distance.

[11] Both dipping interfaces and anisotropy cause predictable *Ps* amplitude variation with back azimuth [*Langston*, 1977b; *Cassidy*, 1992; *Levin and Park*, 1997a, 1997b, 1998; *Savage*, 1998]. For anisotropy with a horizontal symmetry axis, the amplitude of *Ps* horizontal motion is four-lobed with back azimuth, so that the transverse RF vanishes for *P* arrivals parallel and normal to the axis of symmetry. This pattern is easily distinguished from the two-lobed amplitude pattern caused by a dipping interface in isotropic media. For anisotropy with a tilted axis of symmetry, the *Ps* amplitude pattern can be a mixture of four-lobed and two-lobed polarity patterns, depending on the tilt and the ratio of $V_S$ and $V_P$ anisotropy [*Levin and Park*, 1998]. In some cases the effect of a tilted axis of symmetry on transverse RFs resembles that caused by a dipping interface in isotropic media. Anisotropy is indicated if the *Ps* amplitudes are too large to model with a realistic dip angle, e.g., the dip of the Wadati-Benioff zone [*Savage*, 1998].

[12] Bin-averaged radial RFs for station COR (Figure 3) show a strong positive *Ps* conversion at 5.5–6.5 s, which we designate ($P_J s$). $P_J s$ is preceded by a negative *Ps* conversion over a broad back azimuth range. We identify this converted phase doublet with the top of the subducting Juan de Fuca plate. The transverse RFs show a strong converted phase doublet at the same delay time, also with a derivative pulse shape i.e., paired pulses of opposite polarity. The polarities of the transverse component *Ps* conversions switch with back azimuth: positive-to-negative for the downdip sector (60°–180° back azimuth), and negative-to-positive for the updip sector (180°–300° back azimuth). A distinct polarity change for this derivative phase occurs near 180° back azimuth.

[13] For both radial and transverse RFs, the $P_J s$ delay times vary with back azimuth consistent with a dipping Juan de Fuca slab (Figure 3). We observe larger $P_J s$ delay times for arrivals from the downdip side (45°–135° back azimuth) and smaller $P_J s$ delay times for arrivals from the updip side (225°–315° back azimuth). The earthquakes offer two narrow sectors (120°–135° and 295°–310°) in which the moveout of *Ps* with epicentral distance confirms the dipping character of the interface. Fermat's Principle of Least Time causes the *Ps* conversion point on a dipping interface to shift updip, relative to the conversion point on a horizontal interface. This effect increases the *Ps* moveout with epicentral distance on the downdip side (Figure 4) and decreases the moveout on the updip side (Figure 5).

[14] For station COR, the dip of the subducting Juan de Fuca plate is roughly eastward. If an isotropic tilted

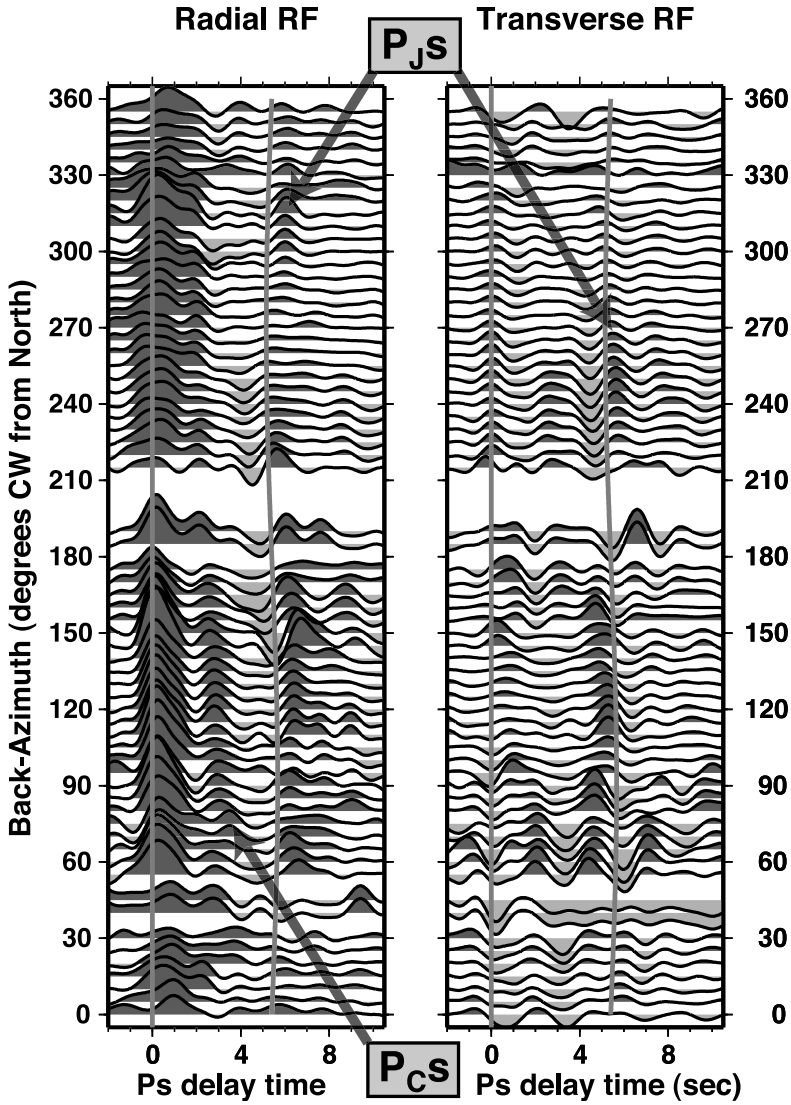


**Figure 3.** Back azimuth receiver function sweeps for station COR. (left) Radial RFs. (right) Transverse RFs. Overlapping stacking bins are 10° wide in back azimuth, spaced by 5°. The RFs are limited to $f < 1.0$ Hz, stacked by bins and low passed in the frequency domain with 0.5-Hz half amplitude to suppress Gibbs effect ringing. The converted phases $P_Cs$ (crustal) and $P_Js$ (Juan de Fuca) are marked. Vertical lines identify both zero delay and the delay of a *Ps* converted wave from an incident *P* wave (phase velocity 20 km/s) at an interface that dips to the east by 15. (The phase velocity 20 km/s is appropriate for epicentral distance $\Delta \sim 78°$.) See color version of this figure in the HTML.

interface alone were responsible for $P_Js$ on the transverse RFs, events from the north would generate negative polarity $P_Js$, and events from the south would generate positive polarity $P_Js$, provided that velocity increases downward. The COR receiver functions do not show this pattern. Instead, the polarity flip on the observed transverse RFs lies along a north-south axis. The $P_Js$ phase on the radial RFs has larger amplitude near the polarity flip, which is consistent with anisotropy. In addition, the transverse RFs have an asymmetric amplitude pattern that suggests the influence of a cos 2ξ amplitude pattern (four-lobed). For instance, converted wave amplitude is larger in the back azimuth sector 80°–250°, that is, for events from the south. An asymmetric *Ps* amplitude pattern can be matched by hexagonal anisotropy with tilted symmetry axis [*Levin and Park*, 1998]. We conclude that subduction zone dip is a minor factor in the transverse *Ps* polarity and attribute the strong phases to seismic anisotropy near the slab interface.

[15] Crustal *Ps* conversions are also evident in COR RFs. At 0-s to 1-s time delay, the transverse RFs exhibit a derivative pulse waveform with two-lobed polarity in back azimuth, with a gradual polarity transition near 120° back azimuth. Another converted phase, which we label $P_Cs$, has large amplitude at ~2.5 s delay in the radial RFs for the back azimuth sector 60°–180°. For the opposing 210°–270° back azimuth sector, $P_Cs$ arrives at ~2.0-s delay. The $P_Cs$ phase is positive on the transverse RF for 150°–330° back azimuth, and negative for the opposing back azimuth sector. A midcrustal interface in the Siletz terrane, proposed by *Trehu et al.* [1994], is a possible cause for the $P_Cs$ phase.

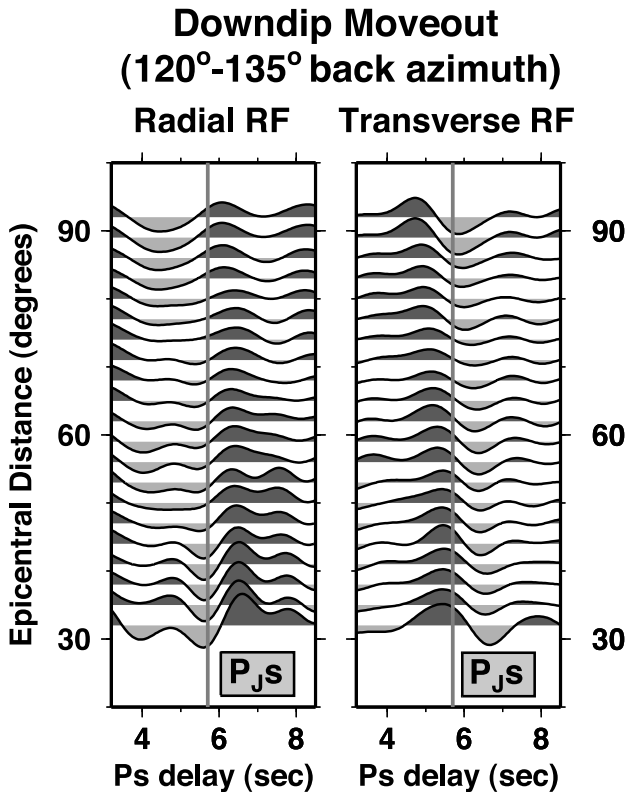


**Figure 4.** Epicentral distance receiver function sweeps for the downdip 120°–135° back azimuth sector at COR. Overlapping stacking bins are 6° wide in back azimuth, spaced by 3°. The eastward dip of the Juan de Fuca plate alters the moveout of the converted phase delay time. For waves that arrive in the downdip sector the moveout of $P_Js$ decreases with increasing epicentral distance. See color version of this figure in the HTML.

A midcrustal anisotropic layer would also help explain a significant feature in the transverse RF at 3.0–3.5 s delay, whose polarity varies in a two-lobed pattern similar to transverse RF features at shorter delay times.

## 4. Tests for the Geometry of Anisotropy

[16] We use a reflectivity algorithm [*Levin and Park*, 1997a] to calculate synthetic seismograms in 1-D horizontally stratified anisotropic structures. The moveout of $P_Js$ makes impossible a perfect phase match between data and 1-D synthetic RFs at a broad range of back azimuth values. The weak slab dip influences the converted wave amplitude, but is not modeled here. We estimate the dip effect on the Ps amplitude more carefully in section 5 with a synthetic seismogram experiment. Results of this experiment argue that 1-D reflectivity modeling is adequate to characterize the major structural features that are expressed in the COR data set.

[17] We assume the anisotropy to have hexagonal symmetry, which implies that an axis of symmetry governs wave propagation effects. Hexagonal symmetry approximates the anisotropy of real rocks, which can be more complex, but the orientation of a symmetry axis can be related more easily to tectonic processes. We use the back azimuth and nominal phase velocity of each event in our data set as input to the synthetic seismogram code, using IASPEI91 as a reference Earth model [*Kennett and Engdahl*, 1991]. We compute RFs from the synthetics with the MTC algorithm, then low-pass filter and bin average these in the same way as the observed RFs. Such mirror processing allows us to match minor variations in the observed *Ps* phase moveout and amplitude.

[18] We compare synthetic with observed RFs for the major phases on both radial and transverse components, and fit the major features of the observations by trial-and-error forward modeling. *Ps* delay times are influenced both by layer thickness and the $V_P/V_S$ ratio (and, equivalently, the Poisson ratio σ). Decreasing $V_P/V_S$ has the same effect on *Ps* delay time as decreasing layer thickness. We constrain $V_P$ and $V_S$ anisotropy to be equal in a percent sense. Numerical tests indicate that $V_P$ anisotropy tends to dominate *P*-to-*S* conversion in media with tilted axis anisotropy. Therefore our data-synthetic comparisons offer weaker constraints on $V_S$ anisotropy than on $V_P$ anisotropy.

[19] We derived an isotropic starting velocity model from *Trehu et al.* [1994], which proposed a mafic crust for the Siletz terrane, with a thin shallow surface layer to simulate sedimentary basins and basement uplifts. These mafic rocks exhibit velocity that ranges between 5.5 km/s in the upper

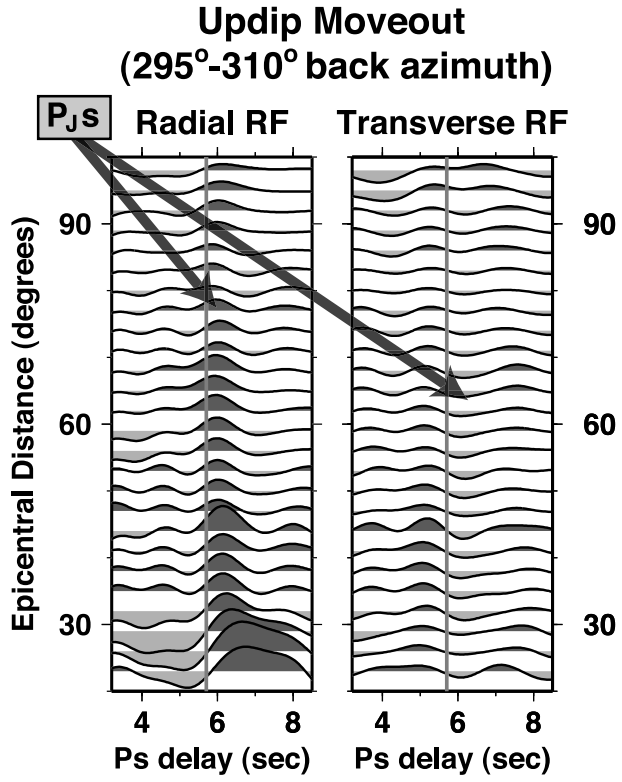


**Figure 5.** Epicentral distance receiver function sweeps for the updip 295°–310° back azimuth sector at COR. Overlapping stacking bins are 6° wide in back azimuth, spaced by 3°. The eastward dip of the Juan de Fuca plate alters the moveout of the converted phase delay time. For waves that arrive in the updip sector, the moveout of $P_Js$ with epicentral distance is suppressed. See color version of this figure in the HTML.

**Table 1.** Anisotropic Velocity Model Consistent With Receiver Functions for Station COR[a]

| Depth, m | $V_P$, m/s | $B$ | $C$ | $V_s$, m/s | $E$ | Density, kg/m$^3$ | Tilt | Strike |
|---|---|---|---|---|---|---|---|---|
| 2,000 | 4650 | −0.08 | 0 | 2700 | −0.08 | 2500 | 45 | 260 |
| 5,000 | 5400 | −0.04 | 0 | 3120 | −0.04 | 2600 | 45 | 200 |
| 9,000 | 6000 | 0 | 0 | 3400 | 0 | 2700 | 0 | 0 |
| 13,000 | 6100 | 0 | 0 | 3400 | 0 | 2700 | 0 | 0 |
| 21,000 | 6600 | 0.03 | 0 | 3600 | 0.03 | 2700 | 40 | 120 |
| 24,000 | 6850 | 0.03 | 0 | 3750 | 0.03 | 2750 | 40 | 120 |
| 36,000 | 7100 | 0 | 0 | 3795 | 0 | 2960 | 0 | 0 |
| 39,500 | 6550 | −0.10 | 0 | 3350 | −0.10 | 2780 | 60 | −5 |
| 43,000 | 6000 | −0.10 | 0 | 2900 | −0.10 | 2600 | 60 | −5 |
| 55,000 | 7100 | 0 | 0 | 3795 | 0 | 2960 | 0 | 0 |
| (half−space) | 8100 | 0 | 0 | 4600 | 0 | 3500 | 0 | 0 |

[a]Depth refers to the base of each layer. The parameters $B$, $C$, and $E$ are coefficients of the $P$ wave cos 2ξ, $P$ wave cos 4ξ, and $S$ wave cos 2ξ anisotropy components, respectively, representing peak-to-peak fractional velocity variation. The quantity ξ is the angle between propagation direction and the axis of symmetry. The sign of $B$ and $E$ is negative for a slow symmetry axis. $B = -0.10$ corresponds to 10% $V_P$ anisotropy with a slow axis of symmetry. The tilt of the symmetry axis is defined as degrees from the vertical. The strike of the symmetry axis is measured as degrees clockwise from north. Adjustments for 10° slab interface dip suggest that the anisotropy between 36 and 43 km depth can be somewhat lower than indicated here, 7% rather than 10%.

crust to more than 7.0 km/s at their greatest thickness of the terrane, ~35 km beneath station COR. *Trehu et al.* [1994] place a low-velocity zone between the base of the Siletz terrane and the Moho of the subducting Juan de Fuca plate. They identify this layer as subducted oceanic crust. *Li* [1996] and *Li and Nabelek* [1996] also identify a low-velocity zone with receiver functions. These researchers chose a high Poisson ratio (σ = 0.33) to represent the Siletz terrane, but aside from serpentinite, most crustal rocks have lower σ. We chose a lower Poisson ratio (σ = 0.28–0.30) for the Siletz terrane to be more consistent with the mafic rock properties [*Christensen*, 1996].

[20] The complexity implicit in the COR RFs motivates a finely layered model (Table 1 and Figure 6) to fit the major observed features (Figures 7 and 8). Aside from its low-velocity layers from 36 to 43 km depth, the isotropic part of this model resembles the starting 1-D model used by *Rondenay et al.* [2001] for this region. In isotropic media, receiver function modeling is vulnerable to trade-offs (e.g., between layer thicknesses and Poisson ratio), so that the uncertainty of seismic velocity in any single layer is large. For anisotropic media, *Ps* polarity and amplitude in the RFs offer supplemental constraints on velocity and anisotropy contrasts at interfaces. In practice, random noise in the amplitudes of the bin-averaged RFs limits the precision of estimated model parameters. Nevertheless, the major features of the COR receiver functions demand large contrasts in model properties, so that the overall interpretation is less vulnerable to formal parameter uncertainties.

[21] Our preferred model has a thin layer of depressed wave speed at 40 km depth with $V_P$ = 6.0 km/s, high Poisson ratio (σ = 0.33) and strong anisotropy (10%) with a slow axis of symmetry tilted 60° from the vertical. Identical anisotropy resides also in a thin transitional layer at the top of the depressed wave speed layer. These two layers cause the slab-related *Ps* waves at 4.5–6.5 s delay. Beneath this layer lies a 12-km layer with wave speed characteristic of gabbroic ocean crust ($V_P$ = 7.1 km/s). The gabbroic layer is motivated by a positive polarity pulse that follows $P_fs$ in most back azimuth sectors. The timing of this pulse, relative to $P_fs$, constrains the thickness of the layer, which is some 50% greater than ordinary oceanic crust.

[22] In the crust of the overriding Siletz terrane, velocities imply gabbroic composition, except for the top few kilometers. A very strong (8%) anisotropy with a tilted slow symmetry axis characterizes a low-velocity surface layer. Shallow anisotropy is motivated by the zero delay pulse on the transverse RF. In synthetic RFs, the reverberations in this layer mimic the behavior of the $P_Cs$ phase at 2.0–2.5 s delay in the observed radial RFs. *Ps* pulses in the first few seconds of the transverse RFs appear to suffer gradual moveout with back azimuth. We can model the "cork-

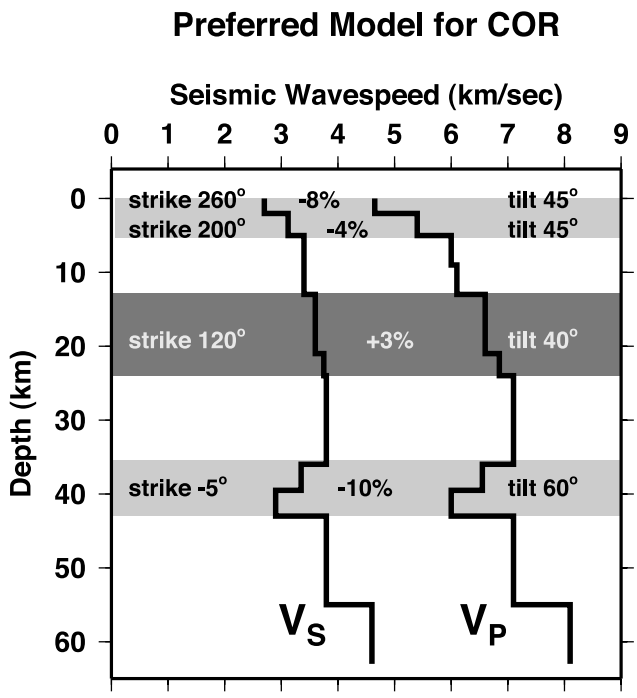


**Figure 6.** Vertical profile of the preferred 1-D anisotropic model beneath Corvallis, Oregon. Shaded zones mark the anisotropic layers. The magnitude (in percent), azimuth (clockwise from north), and tilt angle (from the vertical) of the anisotropy are shown within the zones. The $V_P$ profile is fit to the radial RFs starting from an initial model derived from *Trehu et al.* [1994] and *Li* [1996]. Note the large north trending slow axis anisotropy that resides in a low-velocity layer at the base of the overriding plate. See color version of this figure in the HTML.

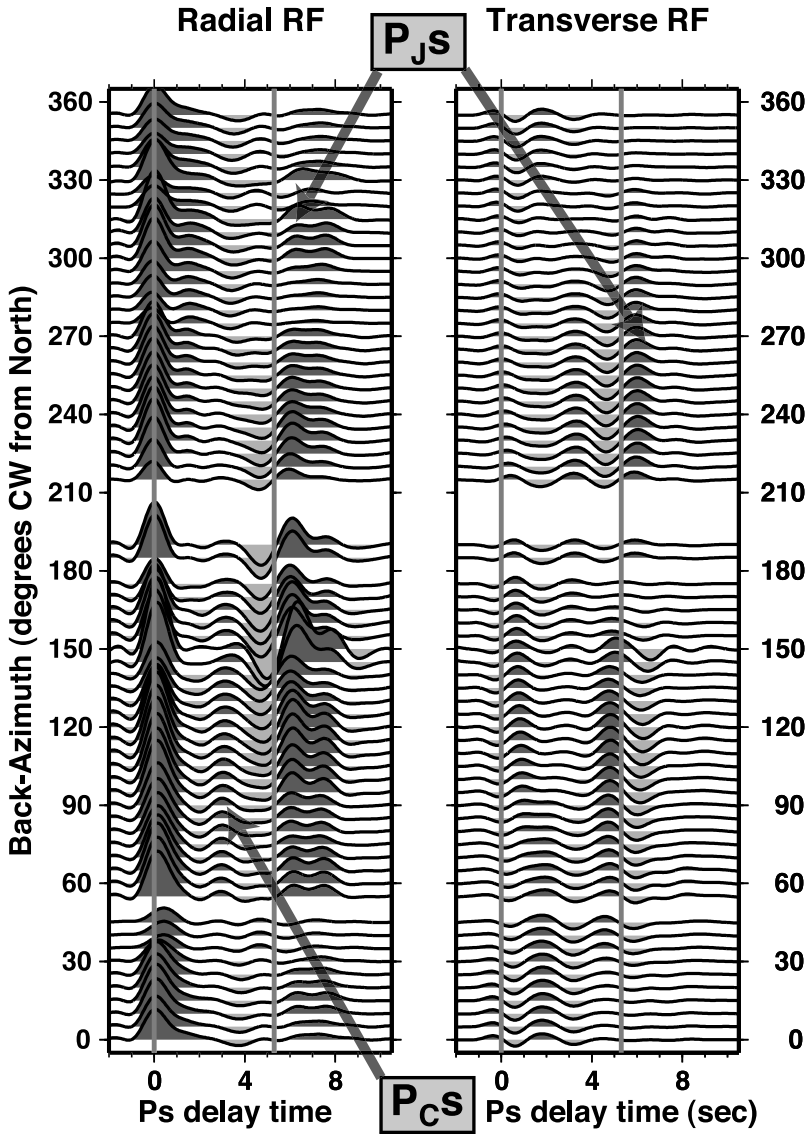


**Figure 7.** Synthetic back azimuth receiver functions for our preferred 1-D anisotropic velocity profile. The RFs are computed from reflectivity synthetics that match the distribution of 602 earthquakes in the data analysis. This strategy helps to match isolated variations in the amplitude and moveout of the observed RFs, displayed in Figure 3. (left) Radial RF sweep. (right) Transverse RF sweep. The RFs are band limited at 1 Hz and low-passed in the frequency domain with 0.5-Hz half amplitude to suppress Gibbs effect ringing. Overlapping stacking bins are 10° wide in back azimuth, spaced by 5°. See color version of this figure in the HTML.

screw'' pattern in this moveout (Figure 3) with a second surface layer (2–5 km depth) whose anisotropic slow axis is rotated 60° counterclockwise (CCW) of the surface layer axis. Weaker anisotropy in the midcrust is motivated by back azimuth-dependent pulses at 2.5–3.5 s delay in the transverse RFs. The symmetry axes of midcrustal anisotropy align with E30°S (120° strike), which does not align with either the inferred anisotropy above the Juan de Fuca slab or with the subduction direction.

[23] Figure 8 offers trace-by-trace comparisons of the observed and modeled bin-averaged receiver functions at COR for two opposing back azimuth bins. Disagreement in the timing of $P_Js$ arises from our modeling a dipping interface with a 1-D structure, but the agreement in amplitude is encouraging. The transverse amplitude of the slab-converted *Ps* phases is as large as the radial amplitude. Far too large to be modeled as a ray deflection from a shallow dipping interface, the amplitude of the transverse RF motivates the 10% anisotropy in our preferred model.

[24] Our forward modeling strategy has the disadvantage that models distinct from our preferred model might fit the data as well, but are not explored. An advantage of forward modeling, on the other hand, is the ability to test and reject alternate models that are tectonically plausible. For instance, the slow axis of symmetry in the deep anisotropic layer of our preferred model fits both the polarity behavior of the transverse RFs and the larger *Ps* amplitudes seen at southerly back azimuths (90°–270°). A fast symmetry axis with

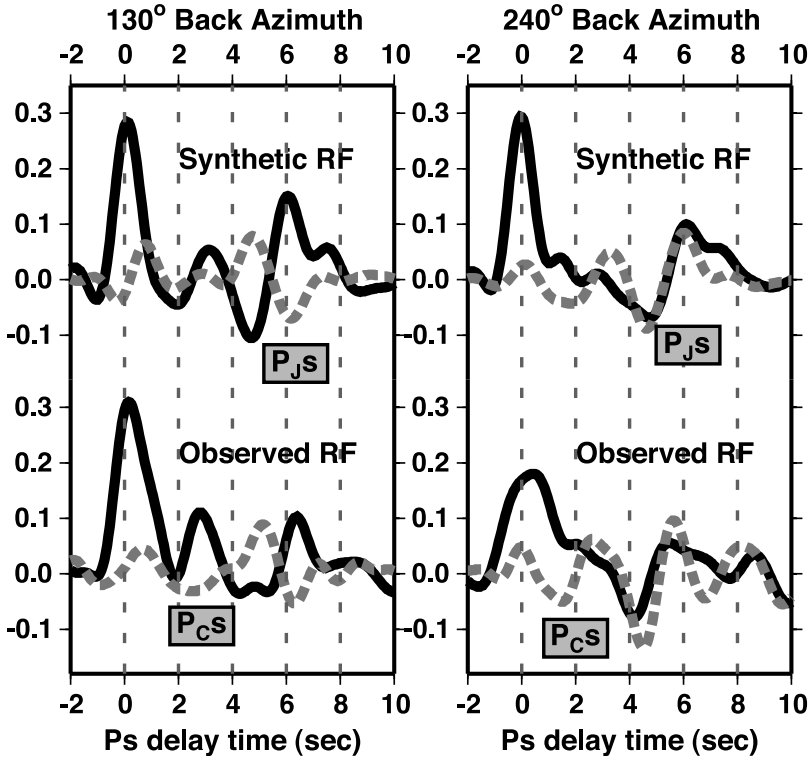


**Figure 8.** Synthetic versus observed receiver functions for averaged back azimuth sectors centered on 130° for (left) downdip sector and on 240° for (right) updip sector. Radial RFs (red) are superimposed on transverse RFs (green). The phase mismatch for the $P_J s$ phase at ~6-s time delay is caused by slab-dip moveout. See color version of this figure in the HTML.

the same orientation would misfit the polarities on the transverse RFs. A fast symmetry axis can be chosen with an orientation (60° tilt, S5°E strike) that fits the observed transverse polarities, but it predicts largest radial $P_J s$ amplitude at northerly back azimuths. A more complicated anisotropic geometry (e.g., orthorhombic symmetry) might fit the data adequately, but we did not explore such models.

[25] Figures 9 and 10 show bin-averaged receiver function sweeps for two variations of our preferred model. The first alternate model (Figure 9) has subduction-parallel horizontal alignment in the low-velocity zone above the slab, and no midcrustal anisotropy. This alternate slab-related anisotropy fails (badly) to explain the observations in two ways. First, subduction alignment with a horizontal symmetry axis induces a four-lobed polarity in the transverse RFs with a node at roughly N68°E. The observed transverse RFs are more two-lobed, with a polarity flip that we observed to lie at N5°W. Second, the *Ps* converted wave amplitude for a horizontal axis of symmetry is too small, even with 10% anisotropy, to match the observations. A tilted axis of symmetry enhances the conversion of *P* waves to *S* significantly, and fits better the back azimuth pattern in the data. We conclude that anisotropy that follows the geometry of large-scale plate motion fails to explain our observations.

[26] Figure 9 shows that the absence of midcrustal anisotropy weakens greatly the $P_C s$ phase at 2.0–2.5 s delay in the radial RFs. Perhaps a surface layer reverberation could explain a larger portion of this feature in the observed RFs, with the proper choice of parameters. However, reverberations in the shallow surface layer do not seem able to explain observed waveforms on the transverse RFs at longer delay times. This supports the case for anisotropy in the midcrust. We note that the depth range and geometry (i.e., slow or fast axis) of the midcrustal anisotropic layer are not constrained in a definitive manner.

[27] Our second alternate model exhibits a seismic velocity ($V_P$ = 6.5 km/s) and Poisson ratio ($\sigma$ = 0.30) in the deep anisotropic layer that would imply a hydrated gabbroic composition, placing it directly above the ultramafic mantle of the Juan de Fuca slab ($V_P$ = 8.1 km/s) and beneath the unmetamorphosed gabbro ($V_P$ = 7.1 km/s) of the Siletz crust. This alternate model aligns its crustal anisotropy with the roughly north-south strike of its slab-related anisotropy. However, the synthetic radial RFs of the second alternate model lack the *Ps* phase that trails $P_J s$ in the observations. Synthetic radial receiver functions for this alternate model do not predict negative polarity for $P_J s$ in any back azimuth sector, consistent with the COR data, but weak amplitude persists in much of the 300°–360° back azimuth sector (Figure 10). The polarity of the *Ps* conversion from the top of the low-velocity zone is negative over a smaller range of back azimuth in the radial RFs than is observed, suggesting that the velocity inversion associated with hydrated oceanic crust is insufficient by itself to model the Corvallis RFs.

[28] In another synthetic experiment (not shown) we examined a model with an unmetamorphosed gabbroic layer ($V_P$ = 7.1 km/s) surrounded below and above by peridotite mantle ($V_P$ = 8.1 km/s). Previous studies [e.g., *Trehu et al.*, 1994] have not suggested that a layer of peridotite lies

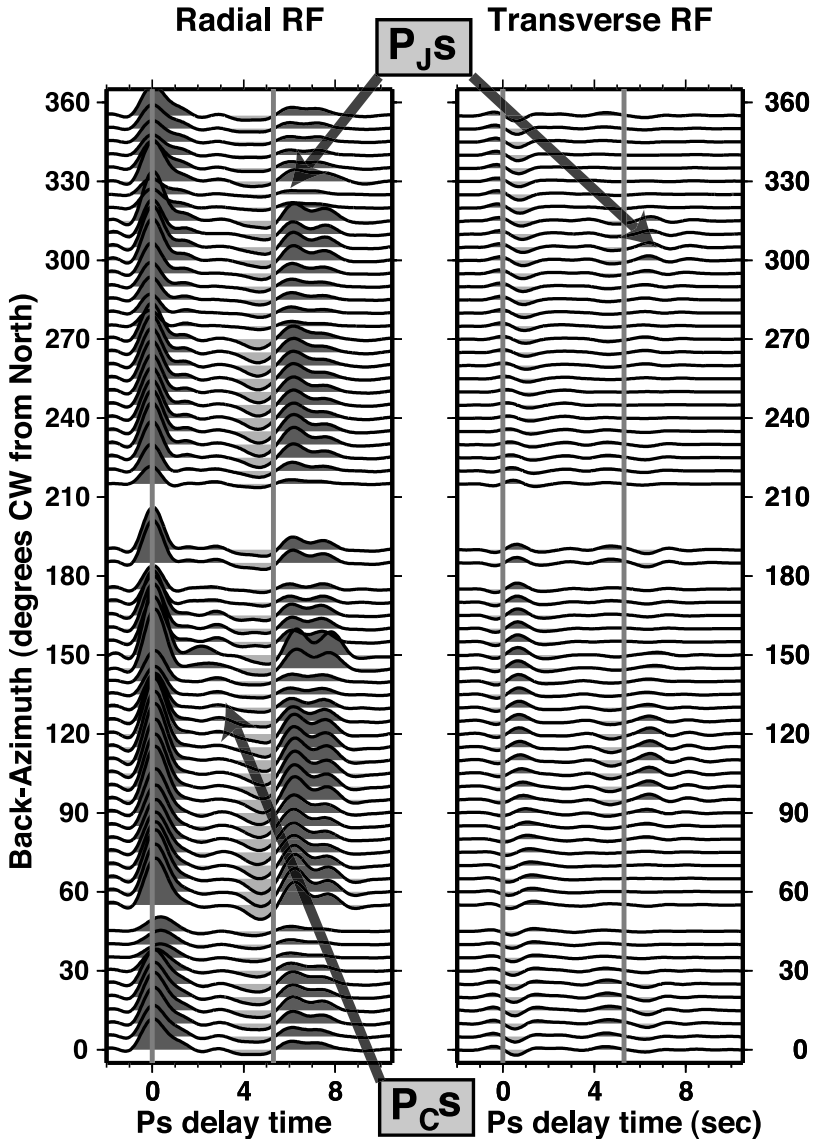


**Figure 9.** Synthetic receiver functions for a model that is tectonically plausible but that does not predict the observations well. We test here a anisotropic model with (1) no midcrustal anisotropy and (2) a horizontal slow symmetry axis in the deep low-velocity zone that aligns with the Cascadia subduction direction (N68°E). The synthetic transverse RF amplitude (too small) and back azimuth variation (four-lobed and misaligned) do not match the slab-related conversions of the observed transverse RF sweeps. See color version of this figure in the HTML.

above the Juan de Fuca slab at this point of the Cascadia subduction zone. The synthetic RFs for such a model also do not suggest the existence of a supraslab peridotite layer at Corvallis. In addition to the shortcomings evident in Figure 10, this model has a Moho in the Siletz terrane that predicts a *Ps* conversion at ~3-s delay with uniformly positive polarity on the radial RF. Such a phase is not observed in data.

[29] Our forward modeling suggests some generalizations. If anisotropy is large, a weak low-velocity zone loses its velocity inversion for some back azimuths. Forward modeling suggests that the $V_S$ profile is more important than the $V_P$ profile in controlling the polarity of the *Ps* conversion in the radial RF. To avoid radial $P_Js$ polarity switches with back azimuth, our "preferred" model has $V_P$ = 6.0 km/s and $\sigma$ = 0.33 for the deep anisotropic layer. Our interpretation follows from associating the Juan de Fuca Moho with a positive polarity *Ps* pulse that arrives $\gtrsim$1 s after the prominent $P_Js$ conversion. We associate the $P_Js$ conversion with the top of the slab, marking the lower boundary of a low-velocity zone of highly sheared hydrated rock. If this low velocity zone had Poisson ratio consistent with either a mafic ($\sigma$ = 0.28–0.30) or felsic ($\sigma$ = 0.25) lithology, one must specify $V_P$ < 6.0 km/s in order to maintain constant $P_Js$ polarity.

[30] Figure 10 also shows that north-south alignment in crustal anisotropy does not fit the observations well. The CCW rotation with depth of the shallow anisotropy in our preferred model, though probably uncertain by 20° or so, does not relate simply to the slab-related anisotropy or the

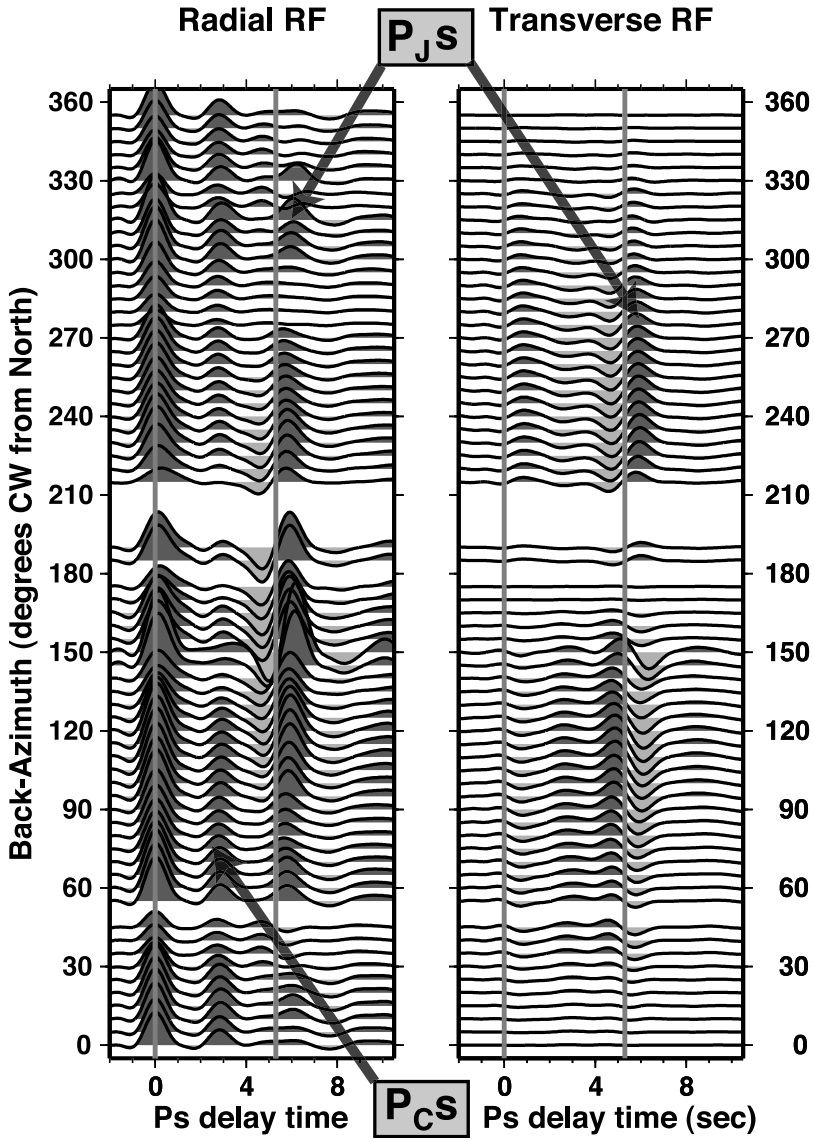


**Figure 10.** Synthetic receiver functions for a model that is tectonically plausible but that does not predict the observations well. We test here a anisotropic model with all crustal anisotropy aligned north-south (to match the geometry of the deeper anisotropy) and a low-velocity zone of hydrated oceanic crust ($V_P$ = 6.5 km/s; $\sigma$ = 0.30) above peridotite ($V_P$ = 8.1 km/s). At short time delay (<3 s) the synthetic RFs for this model do not match the moveout (with back azimuth) of the observed transverse RFs. The positive slab-related $P_Js$ phases on the synthetic radial RFs do not reverse polarity with back azimuth, in agreement with data. However, the radial *Ps* conversion at 4.5–5.0 s delay from the top of the low-velocity layer is negative only at 90°–270° back azimuths, which disagrees with data (Figure 3) and our preferred model (Table 1 and Figure 7). Note that radial RFs for this model lack a positive *Ps* pulse that arrives ~1 s after $P_Js$, which in our preferred model corresponds with the oceanic Moho of the Juan de Fuca plate. See color version of this figure in the HTML.

subduction direction. Overall, our experiments with crustal parameters discourage the possibility the crust beneath Corvallis is much simpler than our preferred model. A crustal model with some other complexity e.g., different layering, orthorhombic symmetry, or 3-D structure, cannot be ruled out.

[31] Synthetic modeling suggests that the orientation of anisotropy appears to be constrained well by polarity flips in the transverse RF. The unusual velocities of the layer we interpret to lie above the slab are based on the lack of polarity changes in $P_Js$ in the radial RF. It is reasonable to question whether $P_Js$ amplitude variations associated with the known dip of the Cascadia slab exert a significant influence on the observed RFs and on our interpretation of them. Synthetics for a fully 2-D model [e.g., *Frederiksen and Bostock*, 2000] could estimate $P_Js$ amplitude and delay time perturbations simultaneously. However, a simple ray-based calculation of *Ps* timing represents well the small expected fluctuations in $P_Js$ delay time in Figure 3, so we chose to estimate $P_Js$ amplitude fluctuations separately with

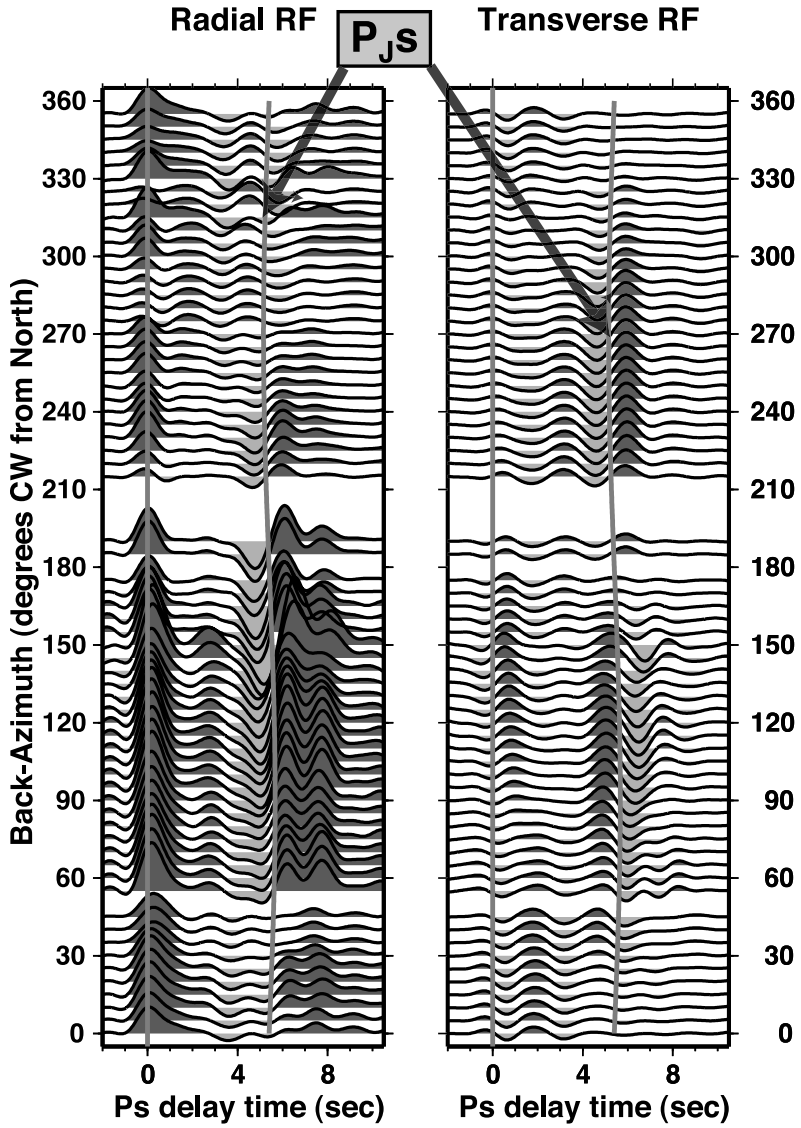


**Figure 11.** Synthetic back azimuth receiver functions for our preferred 1-D anisotropic velocity profile, using perturbations to *P* wave incidence angle to represent the effects of a weakly dipping (10) slab interface on $P_Js$ amplitude. The RFs are computed from reflectivity synthetics that match the distribution of 602 earthquakes in the data analysis. (left) Radial RF sweep. (right) Transverse RF sweep. The synthetic RFs are low-passed to match the bandpass of the observed RFs. Overlapping stacking bins are 10° wide in back azimuth, spaced by 5°. Comparison with Figure 7 argues that the effect of slab dip on the transverse RF polarity is negligible but $P_Js$ amplitude is magnified. Perturbations to $P_Js$ in the radial RF are more significant. The $P_Js$ amplitude is larger for westerly (downdip) back azimuths and changes polarity at northwesterly back azimuths. A decrease of anisotropy in the supraslab depressed wave speed layer from 10% to 7%, leaving other parameters unchanged, can facilitate better agreement between observed RFs (Figure 3) and dipping interface synthetics (not shown). See color version of this figure in the HTML.

an adjustment to 1-D reflectivity. We recomputed reflectivity *P* wave synthetics for 602 events in our COR data set using our preferred anisotropic model with an imposed perturbation to the angle of incidence, appropriate for an interface with 10° east plunging dip. In this approximation, we add 10° to the angle of incidence for an event at 90° back azimuth (downdip), subtract 10° from the angle of incidence for an event at 270° back azimuth (updip), and make intermediate adjustments at other back azimuths. Our approximation induces a bias in the angle of incidence at the free surface, but this bias should be smaller, in a relative sense, than the effect of dip on the *P*-to-*S* converted phase. Figure 11 shows the results of this exercise.

[32] Comparison of Figures 3, 7, and 11 suggests that the predicted effects of slab dip on $P_Js$ amplitude are discernible and can influence the interpretation of the observed RFs. The dip magnifies radial $P_Js$ amplitude for easterly (downdip) back azimuths (0°–180°) (Figure 11) and induces a polarity reversal for *Ps* waves that arrive from the northwest. *P* waves approach the Cascadia slab from the downdip

side at a larger angle to the interface normal and suffer a larger $P_fs$ conversion on the radial RF. The polarity pattern of $P_fs$ in the transverse RFs is unaffected, but $P_fs$ amplitude increases.

[33] On the basis of the dipping interface simulation, it appears that the major features of observed RFs at COR cannot be explained as artifacts of *Ps* conversions at a dipping slab interface. The orientation of anisotropy in the supraslab layers appears to be robust to dip effects. Our inference of unusually low $V_P$, and possibly serpentinite lithology, in the supraslab layer is motivated by the uniform polarity of $P_fs$ with back azimuth in the radial RFs. The effect of slab dip on radial $P_fs$ appears to make the need for a low-$V_P$ layer more acute. The other adjustable parameter is supraslab anisotropy, which overpredicts the transverse $P_fs$ amplitude. If we reduce the anisotropy in the supraslab layer from 10% to 7% in the dipping slab scenario (not shown), we can rectify the reversed radial $P_fs$ polarity for northwestern back azimuths and obtain better agreement with the transverse RFs. A steeper slab dip might be accommodated by a further decrease in supraslab anisotropy, but previous studies suggest that slab dip $\lesssim 20°$. Even with this adjustment to the 1-D structure in Table 1, our modeling still favors the presence of a thin, highly anisotropic low-wave speed layer atop the Cascadia slab beneath station COR with an apparent north-south "slow" axis of symmetry.

## 5. Comparison With *SKS* Splitting and $P_n$ Tomography

[34] $P_n$ anisotropy studies [*Hearn*, 1996; *Smith and Ekstrom*, 1999] reveal "fast" propagation parallel to the subduction of the Juan de Fuca plate beneath the northwest Pacific coast. *SKS* splitting for station COR has fast polarization direction N70°E and 1.5-s delay [*Silver*, 1996, Table 1; see also *Schutt and Humphreys*, 2001], also aligned with Juan de Fuca plate motion. To verify the latter published result, we have examined *SKS* splits for COR for selected events in 1990–2000 using the cross-correlation estimator of *Levin et al.* [1999]. Our measured delay times $\delta t$ are smaller than 1.5 s in most cases and there is some scatter in our apparent fast axes that may indicate multilayer anisotropy. Nevertheless, nearly all measured splits can be characterized as trench-normal or trench-oblique, not trench-parallel. The disagreement with our receiver function model is misleading, because the location and thicknesses of our shallow anisotropic layers may explain why they have not been detected by other anisotropic indicators.

[35] It is possible that $P_n$ waves would not sense a strongly anisotropic layer within a buried low-velocity zone, and a simple calculation shows that our model predicts negligible *SKS* birefringence. Since our anisotropic Juan de Fuca crustal layer is only 7 km thick, its shear wave splitting delay $\delta t \approx 0.25$ s. The disagreement in symmetry axis orientation is also misleading. Neither $P_n$ tomography nor *SKS* splitting studies can readily distinguish anisotropic media with fast and slow symmetry axes, as can back azimuthal RF sweeps. The horizontal projection of the trench-"parallel" (N5°W) tilted slow-axis anisotropy that we infer beneath COR has an apparent fast polarization that is roughly trench-perpendicular, and therefore is not strongly at variance with $P_n$ and *SKS* studies. The splitting expected from our proposed anisotropic layer, however, is far too small for explain *SKS* observations. We tested the small splitting prediction by computing reflectivity synthetics for our preferred COR model with upgoing *SV*-polarized waves for the 602 earthquake locations we used at COR. Only a minority of the real earthquakes produced observable *SKS*, so our synthetic data set was unrealistically densely sampled. Even so, splitting estimates on the synthetic *S* waves revealed only modest scatter about 0.25-s splitting delay.

[36] Unexplained *SKS* splitting argues that additional anisotropy with trench-normal fast polarization resides beneath the subducted Moho, but does not possess shallow gradients strong enough to be prominent in the COR receiver functions. Disagreement between the symmetry axes inferred from receiver functions and *SKS* splitting in Kamchatka led *Levin et al.* [2002] and *Park et al.* [2002] to argue for distinct mantle shear flows above and below the subducting slab: trench-normal corner flow above and trench-parallel extension below. We propose an opposite distinction between above and below slab strain in Cascadia: subduction-parallel shear beneath the slab and trench-parallel strain above it.

## 6. Discussion: A Sheared Serpentinite Detachment Zone?

[37] Convergence strain and volatile release may combine to produce highly anisotropic rock in subduction zones. Factors that induce anisotropy include slaty cleavage, schistosity, recrystallization, and oriented faults for the crust [*Babuska and Cara*, 1991]. Oriented cracks and fine layering of different lithologies leads to anisotropy with a slow symmetry axis perpendicular to the average plane of cracks, faults or bedding planes [*Helbig*, 1994]. Volatile release from the slab can produce hydrous mineral assemblages with strong anisotropy. Hydrous minerals with slaty cleavage tend to possess a slow axis of symmetry [*Babuska and Cara*, 1991]. LPO in the antigorite crystal structure of serpentine also exhibits a slow axis of symmetry [*Kern*, 1993]. By contrast, olivine LPO in dry conditions most commonly generates anisotropy with a fast symmetry axis, in the direction of either maximum extension (for modest finite strains) or flow directions (for large strains) [*Zhang and Karato*, 1995; *Zhang et al.*, 2000]. Abundant water can induce olivine LPO with a slow symmetry axis [*Jung and Karato*, 2001].

[38] In a 1-D forward modeling approximation, the $P_fs$ and neighboring phases are represented well with 10% anisotropy for both *P* and *S* waves with a slow symmetry axis tilted 60° to the north. An extension of 1-D modeling to estimate the effects of a 10° slab dip suggests that 7% anisotropy may be adequate to represent the slab-converted phases. With the proper lithology, such values are reasonable. Schists typically contain abundant hydrous minerals and can possess strong anisotropy (up to 20% in rock aggregates) with a slow symmetry axis [*Babuska and Cara*, 1991; *Okaya et al.*, 1995]. Serpentinite rock samples can exhibit similar levels of anisotropy [*Kern*, 1993]. To justify a highly anisotropic model for station SNZO (South Karori, New Zealand), *Savage* [1998] argues that oceanic

crust subjected to blueschist metamorphism possesses high anisotropy.

[39] We infer $V_P$ = 6.0 km/s in the most anisotropic layer of our model for COR, so a simple intercalation of mantle and crustal rocks is not feasible beneath COR, as was suggested by *Levin and Park* [1997b] for a highly anisotropic lower crustal layer in the Paleozoic Urals foredeep. We hypothesize the presence of hydrated metamorphic rocks. Potential lithologies could include subducted sediments or igneous rock units that have been hydrated by water and other volatiles released by the Juan de Fuca slab. Laboratory-determined elasticity of such rocks [*Christensen*, 1965, 1966; *Godfrey et al.*, 2000; *Kern et al.*, 2002] indicates that the metamorphic rocks most likely to derive from subducted sediments, e.g., schists and slates, have strong anisotropy but mean $V_P \geq 6.0$ km/s and typical Poisson ratio $\sigma \leq 0.30$. Only serpentinite (at deep crustal pressures) exhibits $V_P \leq 6.0$ km/s, though not all serpentine samples have been reported to behave this way, see *Kern* [1993]. At face value, our receiver function modeling argues for a massively hydrated serpentinite layer that lies just above the Cascadia slab. This conclusion resembles, but is not equivalent to, the interpretation of *Bostock et al.* [2002] of the scattered wave migration study of *Rondenay et al.* [2001]. *Bostock et al.* [2002] argue for serpentinization of the supraslab mantle wedge from beneath our station COR toward the Cascade Range inland, basing their argument on an unusual pattern of $V_P$ heterogeneity and models of slab dehydration, not a match between their modeled $V_P$ and the $V_P$ of particular rock types. They interpret the low-velocity zone beneath COR to be subducted oceanic crust, not serpentinite.

[40] Closer attention to anisotropic indicators in this region may help resolve this interpretive disagreement. Because our interpretation is based on the inference of unusually low $V_P$ and high $\sigma$ above the slab, it is worth repeating that body wave scattering, the physical mechanism behind both our analysis and that of *Bostock et al.* [2002], is more sensitive to velocity gradients than to absolute $V_P$ and $V_S$. A velocity profile based on scattered wave migration has more uncertainty than a model based on earthquake travel time and/or active source refraction studies. Our inference of $V_P$ in the deep anisotropic layer beneath COR is calibrated by two sets of observations that are not always available for a receiver function study. First, crustal $V_P$ in the Siletz terrane is constrained by active source seismic studies [*Trehu et al.*, 1994]. Second, large *Ps* converted phases on the transverse RF require a large anisotropy in the low-velocity layer beneath the Siletz terrane. This anisotropy is large enough to disrupt the polarity of *Ps* converted phases on the radial RF if mean $V_P$ in the anisotropic zone is insufficiently low. Additional *Ps* conversions on the radial RF provide evidence for mafic subducted oceanic crust beneath the low-velocity layer. We computed synthetic RFs for models where (1) the anisotropic layer has $V_P$ = 7.1 km/s, consistent with mafic lithology (Figure 10), and (2) the anisotropic layer had $V_P$ = 6.0 km/s and Poisson ratio $\sigma$ = 0.25, consistent with schistose/felsic lithology (not shown). In both cases the back azimuth variation of the synthetic radial RFs fit the observed radial RFs significantly less well.

[41] Supporting evidence for a serpentinite layer beneath COR is not definitive, and persuasive tectonic analogs are not yet recognized. Serpentinites are often associated with fault zones and appear to migrate upward within subduction settings in either particle form or as diapirs [*Fryer et al.*, 2000]. In coastal Oregon, serpentinite exposures is not common, but are more common to the south in California (M. Brandon, personal communication, 2003). The provenance of serpentinite in the Cascadia subduction zone, assuming our inferences are correct, differs significantly from its expression in the Izu-Bonin region, as described by *Kamimura et al.* [2002]. Serpentinization of Izu-Bonin mantle-wedge peridotite decreases both its seismic wave speed and its density. This loss of density is hypothesized to induce serpentinite diapirs that are exposed as seamounts on the seafloor near the trench. Serpentinization would occur at greater pressure and temperature beneath COR, and so form the denser antigorite phase of serpentine, rather than the chrysolite phase, as inferred for Izu-Bonin by *Kamimura et al.* [2002]. Last, there is scant evidence in seismic models for mantle-wedge peridotites ($V_P \geq 8.0$ km/s) in the Siletz terrane, either an ultramafic base to the Siletz terrane has been completely serpentinized or else a sliver of serpentinite has migrated trenchward from deeper in the subduction zone.

[42] The case for a serpentinite layer is boosted by the difficulty of matching its seismic properties with another lower crustal rock type. Low velocity, slow axis anisotropy and elevated Poisson ratio could be replicated by a schist with fluid-filled cracks. Such a lithology at these depths is rarely reported, but see *Ague* [1995] for one example.

[43] If a serpentinite layer lies atop the shallow dipping Cascadia slab, the physical consequences could be profound. The rheology of serpentinite favors creep and stable sliding rather than brittle fracture [*Rayleigh and Paterson*, 1965] and has been cited by *Kamimura et al.* [2002] as an important factor in suppressing the occurrence of moderate to large shallow earthquakes in the Izu-Bonin subduction zone. It is tempting to hypothesize that a serpentinite layer in the Cascadia subduction zone, if widespread, could help explain its low level of small to moderate thrust earthquakes (Figure 1) and the occurrence of widespread slow creep events reported by *Miller et al.* [2002].

## 7. Conclusions

[44] Teleseismic receiver functions (RFs) for station COR (Corvallis, Oregon) indicate that the underlying structure is characterized by thin layers (5–10 km) of anisotropic rock; one of these layers is likely associated with a localized shear zone between the downgoing slab and the Siletz forearc terrane. Forward modeling suggests that *Ps* converted phases arise from an anisotropic layer of low wave speed atop the subducted oceanic crust of the Juan de Fuca plate. The Moho of the subducting plate is visible as a less prominent *Ps* converted phase, primarily on the radial component. Back azimuth RF sweeps are consistent with anisotropy that possesses a tilted axis of symmetry, and whose surface projection is roughly trench-parallel. Symmetry axis orientations are consistent with shear associated with a northward migration of the Siletz terrane. The migration of this forearc terrane is evident in GPS measurements [*Mazzotti et al.*, 2002] and could be induced by

oblique subduction [*Yeats et al.*, 1996] or by gravitational collapse of Basin and Range topography [*McCaffrey et al.*, 2000].

[45] Epicentral variation in composite RFs from narrow back azimuth sectors confirms the *Ps* moveout associated with the gentle dip of the Juan de Fuca slab beneath COR. The polarity and amplitude asymmetry of the $P_Js$ converted phase on the transverse RFs argues for anisotropy above the Juan de Fuca Moho with a slow axis of symmetry tilted 60° toward the north. The large anisotropy necessary to model the slab-related phases compels unusually low $V_P$ just above the slab in order to avoid disrupting the polarity of the radial $P_Js$ phase at northerly back azimuths. We hypothesize that metamorphosed mantle rocks (serpentinites) in the depressed wave speed zone above the descending Juan de Fuca Moho are responsible for the strong (10%) anisotropy suggested by 1-D RF modeling. Adjustment in the RF modeling for 10° dip on the Cascadia slab interface suggest that the anisotropy in the supraslab layer may be somewhat lower, perhaps 7%, but still substantial. Hydrated schists, metamorphosed from subducted sediments, could also be responsible, but low $V_P$ in the layer might imply the presence of fluid-filled cracks. For either case, volatile release by the subducting slab has helped to create a highly deformed, hydrated detachment layer within the subduction zone.

[46] **Acknowledgments.** This research was supported by the NSF grants EAR-9805206 and EAR-0106867. We thank Mark Brandon, Jay J. Ague, and Stephan Rondenay for useful comments in the course of this project. Seismic data were obtained from the Data Management System of the Incorporated Research Institutions for Seismology. Station COR is part of the Global Seismographic Network [*Butler et al.*, 2004]. Many figures were prepared with the Generic Mapping Tools of *Wessel and Smith* [1991].

## References

Ague, J. J. (1995), Deep crustal growth of quartz, kyanite and garnet into large aperture, fluid-filled fractures, northeastern Connecticut, USA, *J. Metamorph. Geol.*, *13*, 299–314.

Ague, J. J., and M. T. Brandon (1992), Tilt and northward offset of Cordilleran batholiths resolved using igneous barometry, *Nature*, *360*, 146–149.

Ague, J. J., and M. T. Brandon (1996), Regional tilt of the Mt. Stuart batholith, Washington, determined using Al-in-hornblende barometry: Implications for northward translation of Baja British Columbia, *Geol. Soc. Am. Bull.*, *108*, 471–488.

Ammon, C. J. (1991), The isolation of receiver effects from teleseismic *P* waveforms, *Bull. Seismol. Soc. Am.*, *81*, 2504–2510.

Babuska, V., and M. Cara (1991), *Seismic Anisotropy in the Earth*, Kluwer Acad., Norwell, Mass.

Beck, M. E., Jr. (1984), Has the Washington and Oregon Coast Range moved northward?, *Geology*, *12*, 737–740.

Beck, M. E., Jr. (1989), Paleomagnetism of continental North America: Implications for displacement of crustal blocks within the Western Cordillera, Baja California to British Columbia, in *Geophysical Framework of the Continental United States*, edited by L. C. Pakiser and W. D. Mooney, *Mem. Geol. Soc. Am.*, *172*, 471–492.

Beck, M. E., R. F. Burmeister, and R. Schoonover (1981), Paleomagnetism and tectonics of the Cretaceous Mt. Stuart Batholith of Washington: Translation or tilt?, *Earth Planet Sci. Lett.*, *56*, 336–342.

Bostock, M. G. (1997), Anisotropic upper-mantle stratigraphy and architecture of the slave craton, *Nature*, *390*, 392–395.

Bostock, M. G. (1998), Mantle stratigraphy and the evolution of the Slave province, *J. Geophys. Res.*, *103*, 21,183–21,200.

Bostock, M. G., S. Rondenay, and J. Schragge (2001), Multiparameter two-dimensional inversion of scattered teleseismic body waves: 1. Theory for oblique incidence, *J. Geophys. Res.*, *106*, 30,771–30,782.

Bostock, M. G., R. D. Hyndman, S. Rondenay, and S. M. Peacock (2002), An inverted continental Moho and serpentinization of the forearc mantle, *Nature*, *417*, 536–538.

Burdick, L. J., and C. A. Langston (1977), Modeling crustal structure through the use of converted phases in teleseismic body waveforms, *Bull. Seismol. Soc. Am.*, *67*, 677–691.

Butler, R. F., G. E. Gehrels, W. C. McClelland, S. R. May, and D. Klepacki (1989), Discordant paleomagnetic poles from the Canadian Coast Plutonic Complex: Regional tilt rather than large-scale displacement?, *Geology*, *17*, 691–694.

Butler, R., et al. (2004), The Global Seismographic Network surpasses its design goal, *Eos Trans. AGU*, *85*, 225, 229.

Cassidy, J. F. (1992), Numerical experiments in broadband receiver function analysis, *Bull. Seismol. Soc. Am.*, *82*, 1453–1474.

Christensen, N. I. (1965), Compressional wave velocities in metamorphic rocks at pressures to 10 kilobars, *J. Geophys. Res.*, *70*, 6147–6164.

Christensen, N. I. (1966), Shear wave velocities in metamorphic rocks at pressures to 10 kilobars, *J. Geophys. Res.*, *71*, 3549–3556.

Christensen, N. I. (1996), Poisson's ratio and crustal seismology, *J. Geophys. Res.*, *101*, 3139–3156.

Couch, R., and R. Riddihough (1989), The crustal structure of the western continental margin of North America, in *Geophysical Framework of the Continental United States*, edited by L. C. Pakiser and W. D. Mooney, *Mem. Geol. Soc. Am.*, *172*, 103–128.

Dragert, H., and R. D. Hyndman (1995), Continuous GPS monitoring of elastic strain in the northern Cascadia subduction zone, *Geophys. Res. Lett.*, *22*, 755–758.

Engebretson, D. C., A. Cox, and R. G. Gordon (1984), Relative motions between oceanic plates of the Pacific Basin, *J. Geophys. Res.*, *89*, 10,291–10,310.

Frederiksen, A. W., and M. G. Bostock (2000), Modeling teleseismic waves in dipping anisotropic structures, *Geophys. J. Int.*, *141*, 401–412.

Fryer, P., J. P. Lockwood, N. Becker, S. Phipps, and C. S. Todd (2000), Significance of serpentine mud volcanism in convergent margins, in *Ophiolites and Oceanic Crust: New Insights from Field Studies and the Ocean Drilling Program*, edited by Y. Dilek et al., *Spec. Pap. Geol. Soc. Am.*, *349*, 35–51.

Godfrey, N. J., N. I. Christensen, and D. A. Okaya (2000), Anisotropy of schists: Contribution of crustal anisotropy to active source seismic experiments and shear wave splitting observations, *J. Geophys. Res.*, *105*, 27,991–28,007.

Harris, A. R., H. M. Iyer, and P. B. Dawson (1991), Imaging the Juan de Fuca plate beneath southern Oregon using teleseismic *P* wave residuals, *J. Geophys. Res.*, *96*, 19,879–19,889.

Hearn, T. M. (1996), Anisotropic $P_n$ tomography in the western United States, *J. Geophys. Res.*, *101*, 8403–8414.

Helbig, K. (1994), *Foundations of Anisotropy for Exploration Seismics*, Pergammon, New York.

Hyndman, R. D., C. J. Yorath, R. M. Clowes, and E. E. Davis (1990), The northern Cascadia subduction zone at Vancouver Island: Seismic structure and tectonic history, *Can. J. Earth Sci.*, *27*, 313–329.

Irving, E., G. J. Woodsworth, P. J. Wynne, and A. Morrison (1985), Paleomagnetic evidence for displacement from the south of the Coast Plutonic Complex, British Columbia, *Can. J. Earth Sci.*, *22*, 584–598.

Irving, E., D. J. Thorkelson, P. M. Wheadon, and R. J. Enkin (1995), Paleomagnetism of the Spences Bridge Group and northward displacement of the Intermontane Belt, British Columbia: A second look, *J. Geophys. Res.*, *100*, 6057–6071.

Jung, H., and S.-I. Karato (2001), Water-induced fabric transitions in olivine, *Science*, *293*, 1460–1462.

Kamimura, A., J. Kasahara, M. Shinohara, R. Hino, H. Shiobara, G. Fujie, and T. Kanazawa (2002), Crustal structure study at the Izu-Bonin subduction zone around 31°N: Implications of serpentinized materials along the subduction plate boundary, *Phys. Earth Planet. Inter.*, *32*, 105–129.

Keach, R. W., II, J. E. Oliver, L. D. Brown, and S. Kaufman (1989), Cenozoic active margin and shallow Cascades structure; COCORP results from western Oregon, *Geol. Soc. Am. Bull.*, *101*, 783–794.

Kennett, B. L. N., and E. R. Engdahl (1991), Traveltimes for global earthquake location and phase identification, *Geophys. J. Int.*, *105*, 429–465.

Kern, H. (1993), *P* and *S*-wave anisotropy and shear-wave splitting at pressure and temperature in possible mantle rocks and their relation to the rock fabric, *Phys. Earth Planet. Inter.*, *78*, 245–256.

Kern, H., B. Liu, and T. Popp (1997), Relationship between anisotropy of *P* and *S* wave velocities and anisotropy of attenuation in serpentinite and amphibolite, *J. Geophys. Res.*, *102*, 3051–3065.

Kern, H., Z. Jin, S. Gao, T. Popp, and Z. Xu (2002), Physical properties of ultrahigh-pressure metamorphic rocks from the Sulu terrain, eastern central China: Implications for the seismic structure at the Donghai (CCSD) drilling site, *Tectonophysics*, *354*, 315–330.

Khazaradze, G., A. Qamar, and H. Dragert (1999), Tectonic deformation in western Washington from continuous GPS measurements, *Geophys. Res. Lett.*, *26*, 3153–3156.

Langston, C. A. (1977a), Corvallis, Oregon, crustal and upper mantle receiver structure from teleseismic *P* and *S* waves, *Bull. Seismol. Soc. Am.*, *67*, 713–724.

Langston, C. A. (1977b), The effect of planar dipping structure on source and receiver responses for constant ray parameter, *Bull. Seismol. Soc. Am.*, *67*, 1029–1050.

Langston, C. A. (1981), Evidence for the subducting lithosphere under southern Vancouver Island and western Oregon from teleseismic *P* wave conversions, *J. Geophys. Res.*, *86*, 209–220.

Levin, V., and J. Park (1997a), *P-SH* conversions in a flat-layered medium with anisotropy of arbitrary orientation, *Geophys. J. Int.*, *141*, 253–266.

Levin, V., and J. Park (1997b), Crustal anisotropy in the Ural Mountains foredeep from teleseismic receiver functions, *Geophys. Res. Lett.*, *24*, 1283–1286.

Levin, V., and J. Park (1998), A *P-SH* conversion in a layered media with hexagonally symmetric anisotropy: A cookbook, *Pur. Appl. Geophys.*, *151*, 669–697.

Levin, V., and J. Park (2000), Shear zones in the Proterozoic lithosphere of the Arabian Shield and the nature of the Hales discontinuity, *Tectonophysics*, *323*, 131–148.

Levin, V., W. Menke, and J. Park (1999), Shear wave splitting in Appalachians and Urals: A case for multilayered anisotropy, *J. Geophys. Res.*, *104*, 17,975–17,994.

Levin, V., J. Park, J. Lees, M. T. Brandon, V. Peyton, E. Gordeev, and A. Ozerov (2002), Crust and upper mantle of Kamchatka from teleseismic receiver functions, *Tectonophysics*, *358*, 233–265.

Li, X. Q. (1996), Deconvolving orbital surface waves for the source duration of large earthquakes and modeling the receiver functions for the Earth structure beneath a broadband seismometer array in the Cascadia subduction zone, Ph.D. dissertation, Oreg. State Univ., Corvallis.

Li, X., and J. L. Nabelek (1996), Modeling the structure of the Cascadia subduction zone in Oregon using the receiver functions from a broadband seismometer array (abstract), *Eos Trans. AGU*, *77*(46), Fall Suppl. Meet., F656.

Mazzotti, S., H. Dragert, R. D. Hyndman, M. M. Miller, and J. A. Henton (2002), GPS deformation in a region of high crustal seismicity: N. Cascadia forearc, *Earth Planet. Sci. Lett.*, *198*, 41–48.

McCaffrey, R., and C. Goldfinger (1995), Forearc deformation and great subduction zone earthquakes: Implications for Cascadia offshore earthquake potential, *Science*, *267*, 856–859.

McCaffrey, R., M. D. Long, C. Goldfinger, P. C. Zwick, J. L. Nabelek, C. K. Johnson, and C. Smith (2000), Rotation and plate locking at the southern Cascadia subduction zone, *Geophys. Res. Lett.*, *27*, 3117–3120.

Michaelson, A. C., and C. S. Weaver (1986), Upper mantle structure from teleseismic *P* wave arrivals in Washington and northern Oregon, *J. Geophys. Res.*, *91*, 1094–2077.

Miller, M. M., T. Melbourne, D. J. Johnson, and W. Q. Sumner (2002), Periodic slow earthquakes from the Cascadia subduction zone, *Science*, *295*, 2423.

Okaya, D., N. Christensen, D. Stanley, and T. Stern (1995), Crustal anisotropy in the vicinity of the Alpine Fault Zone, South Island, New Zealand, *N. Z. J. Geol. Geophys.*, *38*, 579–583.

Park, J., and V. Levin (2000), Receiver functions from multiple-taper spectral correlation estimates, *Bull. Seismol. Soc. Am.*, *99*, 1507–1520.

Park, J., C. R. Lindberg, and F. L. Vernon III (1987), Multitaper spectral analysis of high-frequency seismograms, *J. Geophys. Res.*, *92*, 12,675–12,684.

Park, J., V. Levin, M. T. Brandon, J. M. Lees, V. Peyton, E. Gordeev, and A. Ozerov (2002), A dangling slab, amplified arc volcanism, mantle flow and seismic anisotropy near the Kamchatka plate corner, in *Plate Boundary Zones*, *Geodyn. Ser.*, vol. 30, edited by S. Stein and J. Freymueller, pp. 295–324, AGU, Washington, D. C.

Rasmussen, J., and E. Humphreys (1988), Tomographic image of the Juan de Fuca plate beneath Washington and western Oregon using teleseismic *P*-wave travel times, *Geophys. Res. Lett.*, *15*, 1417–1420.

Rayleigh, C. B., and M. S. Paterson (1965), Experimental deformation of serpentinite and its tectonic implications, *J. Geophys. Res.*, *70*, 3965–3985.

Riddihough, R. P. (1984), Recent plate movements of the Juan de Fuca plate system, *J. Geophys. Res.*, *89*, 6980–6994.

Rondenay, S., M. G. Bostock, and J. Schragge (2001), Multiparameter two-dimensional inversion of scattered teleseismic body waves: 3. Application to the Cascadia 1993 data set, *J. Geophys. Res.*, *106*, 30,795–30,807.

Savage, M. (1998), Lower crustal anisotropy or dipping boundaries? Effects on receiver functions and a case study in New Zealand, *J. Geophys. Res.*, *103*, 15,069–15,087.

Schragge, J., M. G. Bostock, and S. Rondenay (2001), Multiparameter two-dimensional inversion of scattered teleseismic body waves: 2. Numerical examples, *J. Geophys. Res.*, *106*, 30,783–30,793.

Schutt, D. L., and E. D. Humphreys (2001), Evidence for a deep asthenosphere beneath North America from western United States *SKS* splits, *Geology*, *29*, 291–294.

Silver, P. G. (1996), Seismic anisotropy beneath the continents: Probing the depths of geology, *Annu. Rev. Earth Planet. Sci.*, *24*, 385–432.

Smith, P. G., and G. Ekstrom (1999), A global study of $P_n$ anisotropy beneath continents, *J. Geophys. Res.*, *104*, 963–980.

Tabor, J. J., and S. W. Smith (1985), Seismicity and focal mechanisms associated with subduction of the Juan de Fuca plate beneath the Olympic Peninsula, *Bull. Seismol. Soc. Am.*, *75*, 237–249.

Thomson, D. J. (1982), Spectrum estimation and harmonic analysis, *IEEE Proc.*, *70*, 1055–1096.

Trehu, A. M., I. Asudeh, T. M. Brocher, J. Leutgert, W. D. Mooney, J. N. Nabelek, and Y. Nakamura (1994), Crustal architecture of the Cascadia fore-arc, *Science*, *265*, 237–243.

Wang, K. (1996), Simplified analysis of horizontal stresses in a buttressed fore-arc sliver at an oblique subduction zone, *Geophys. Res. Lett.*, *23*, 2021–2024.

Wells, R. E. (1990), Paleomagnetic rotations and the Cenozoic tectonics of the Cascade arc, Washington, Oregon, and California, *J. Geophys. Res.*, *95*, 19,409–19,417.

Wells, R. E., C. S. Weaver, and R. J. Blakely (1998), Fore-arc migration in Cascadia and its neotectonic significance, *Geology*, *26*, 759–762.

Wessel, P., and W. H. F. Smith (1991), Free software helps map and display data, *Eos Trans. AGU*, *72*, 441, 445–446.

Yeats, R. S., K. Sieh, and C. R. Allen (1996), *The Geology of Earthquakes*, Oxford Univ. Press, New York.

Zhang, S., and S. Karato (1995), Lattice preferred orientation of olivine aggregates deformed in simple shear, *Nature*, *375*, 774–777.

Zhang, S., S.-I. Karato, J. FitzGerald, U. H. Faul, and Y. Zhou (2000), Simple shear deformation of olivine aggregates, *Tectonophysics*, *316*, 133–152.

V. Levin, Department of Geological Sciences, Rutgers University, 610 Taylor Road, Piscataway, NJ 08854, USA. (vlevin@rci.rutgers.edu)

J. Park, Department of Geology and Geophysics, Box 208109, Yale University, New Haven, CT 06520-8109, USA. (jeffrey.park@yale.edu)

H. Yuan, Department of Geology and Geophysics, University of Wyoming, 1000 E. University Avenue, Laramie, WY 82071, USA. (yuan@uwyo.edu)